Efficient Energy Transfer between Laser Beams by Stimulated Raman Scattering

Youbo Zhao, Tana E. Witt, and Robert J. Gordon

Department of Chemistry, University of Illinois at Chicago, Chicago, Illinois 60680-7061, USA

(Received 2 May 2009; published 23 October 2009)

Efficient energy transfer between two ultrafast laser beams is reported. Energy transfer occurs when linearly polarized donor and acceptor beams are focused in air and intersect at an acute angle. This effect is attributed to plasma-mediated forward stimulated Raman scattering, facilitated by supercontinuum generation. Donor depletion as high as 57% is observed, with quantitative energy transfer from the donor to the acceptor beam. Amplification of the acceptor depends on the polarization directions of the two pulses and the delay between them. Interaction between the beams results also in compression and spectral broadening of the acceptor pulse.

DOI: 10.1103/PhysRevLett.103.173903 PACS numbers: 42.65.Dr, 42.79.Ta, 52.38.-r

All-optical control of light propagation is of broad interest in science and engineering, with application to areas such as photonic computing, optical communication, ultrafast spectroscopy, and laser amplification [1–7]. An example is the optical Kerr effect [8], in which a pulse of light induces birefringence in a medium, thereby allowing a linearly polarized light beam to pass through a pair of crossed polarizers. Electromagnetically induced transparency [9] occurs when quantum interference induced by a control beam reduces the absorption of light tuned to a resonance frequency of the medium. The group velocity of light may be slowed by using a control beam to induce a steep change in the refractive index of the medium [10]. Four wave mixing occurs when a pair of light beams create an optical grating, which scatters a third beam [11].

In all these examples, one or more light beams modify the optical properties of a medium so as to control the propagation of an independent probe beam. It is also possible to take a more active approach in which one beam transfers a substantial fraction of its energy to a second beam. Many studies have been performed using backwards stimulated Raman scattering (SRS), in which two beams counterpropagate over a distance of several mm through a preformed plasma [12]. Much higher transfer efficiencies of low energy pulses have been achieved in fibers on a length scale of meters [13]. In another two-beam coupling scheme, a pair of laser pulses intersect at a grazing angle to produce a dynamic phase grating in the resulting filaments, which promotes energy transfer between the beams [14].

Here we report a simple and robust method of transferring most of the energy from one laser to another on a fs time scale over a distance of tens of μm by simply focusing and intersecting them in air. Two linearly polarized Ti:sapphire laser beams (790 nm, 50 fs) intersect at an angle θ [Fig. 1(a)]. Near their focal points the intensity of each is sufficient to ionize the air, producing the trails shown in Fig. 1(b). If the beams intersect without overlapping temporally, they simply pass through each other. If the pulses are timed, however, to collide at the crossing point, a large fraction of the energy from the one pulse (the "donor") is transferred to the other ("acceptor") pulse. The crossing point lies before the focus of the donor and after the focus of the acceptor laser. The donor and acceptor beams are focused with plano-convex lenses having focal lengths of 150 and 100 mm, producing $1/e^2$ beam waists of 28 and 20 μm and Rayleigh lengths of 920 and 420 μm, respectively. The images in Fig. 1 were collected with a 4x objective and detected with a CCD camera.

The energy transfer efficiency was found to depend on the intensities of the lasers, the location, angle, and timing of their intersection, and their polarizations. As shown in Fig. 2(a), the output energy of the acceptor pulse, $E_{a,o}$, increases with its initial energy, $E_{a,i}$, whereas the gain ratio G (defined as the ratio of $E_{a,o}$ with and without the donor pulse present) decreases with $E_{a,i}$. As shown in the inset of Fig. 2(a), G falls off at low values of $E_{a,i}$, as must be the case near the threshold for air breakdown. The decline in G

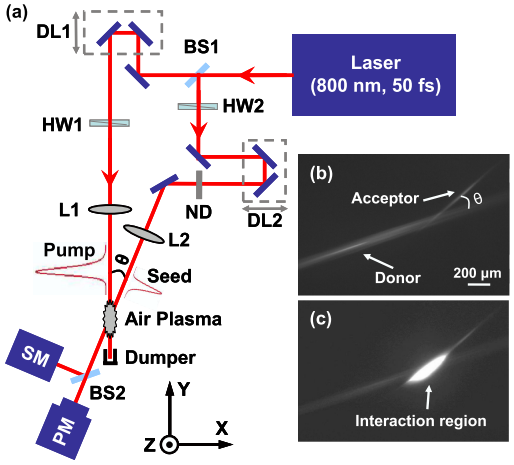

FIG. 1 (color online). Experimental setup (a) and images of the plasmas produced by the intersecting lasers, with (b) 100 fs and (c) zero delay between the pulses. Apparatus components include lenses (L1, L2), half wave plates (HW1, HW2), beam splitters (BS1, BS2), delay lines (DL1, DL2), a neutral density filter (ND), a power meter (PM) and spectrograph (SM).

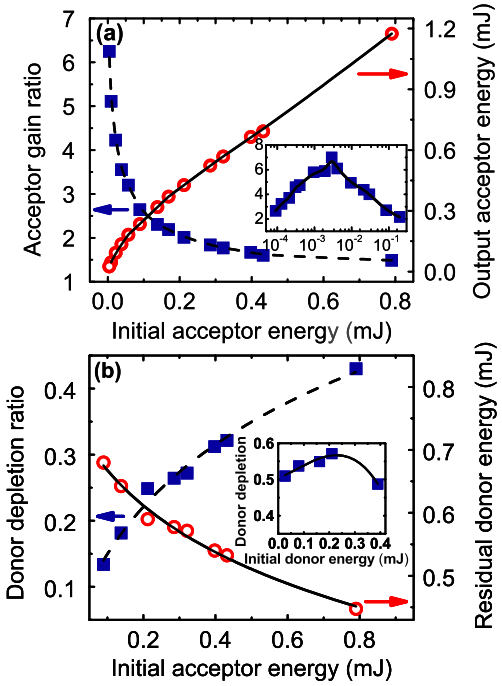

FIG. 2 (color online). Dependence of the energy transfer efficiency on the initial donor energy. (a) Acceptor energy gain ratio (squares) and energy of the amplified acceptor pulse (circles). (b) Fraction of the donor energy depleted by the acceptor (squares) and the residual energy of the donor pulse (circles). The inset in (b) shows the depletion fraction as a function of $E_{d,i}$ with $E_{a,i} = 790$ μJ.

at large $E_{a,i}$ could be caused by a wave-breaking mechanism [15]. The energy loss of the donor is shown in Fig. 2(b). We find that the depletion fraction D increases with $E_{a,i}$, with 43% depletion occurring at an $E_{a,i} = 790$ μJ. From this trend, even greater depletion is expected at higher acceptor energies. Since greater pulse energies were not available with our apparatus, we decreased $E_{d,i}$ while maintaining $E_{a,i} = 790$ μJ, so as to obtain higher acceptor/donor ratios. As shown on the inset to Fig. 2(b), 57% of the energy was transferred when $E_{d,i}$ was decreased to 210 μJ.

Figure 3 shows some of the effects of the spatial and temporal properties of the laser beams. In panel (a), the donor is polarized in a plane normal to the plane of intersection of the two beams (s polarization), while the acceptor polarization vector is rotated by an angle of α with respect to the donor polarization. We observe quantitative energy transfer from one beam to the other, with maximum energy transfer occurring when the polarization vectors are parallel ($\alpha = 0$) and minimum transfer when they are perpendicular to each other. Panel (b) shows the dependence of G on θ for both p and s polarization. At each angle, the crossing point was adjusted to maximize the energy transfer. We see that G falls dramatically as the scattering shifts from forwards to backwards, with greater amplification for s polarization. Finally, in panel (c) we examine the effect of a time delay between the two pulses.

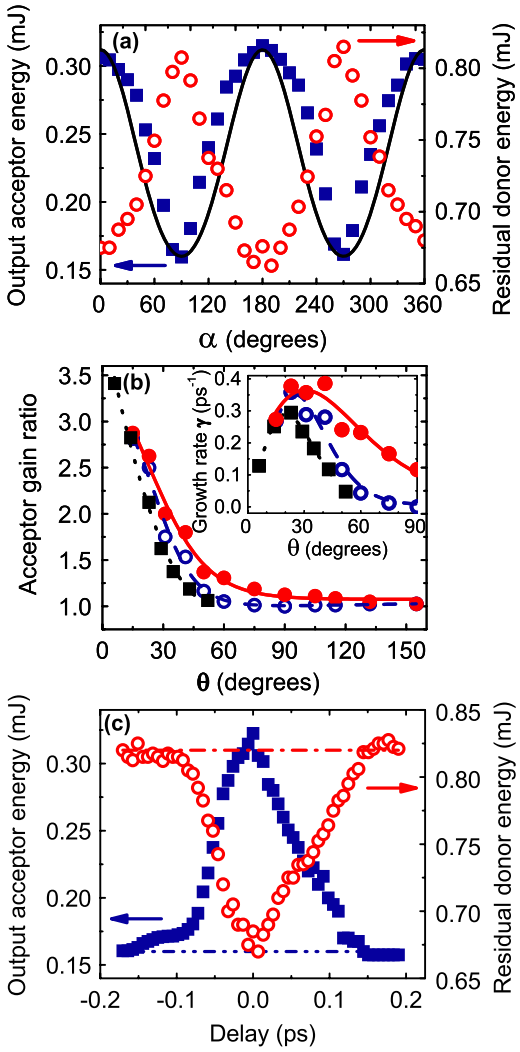

FIG. 3 (color online). Dependence of $E_{a,o}$ and $E_{d,o}$ on the spatial and temporal properties of the intersecting lasers. (a) Donor (open symbols) and acceptor (solid symbols) output energies as functions of the angle between their polarization vectors, α, with $E_{d,i} = 820$ μJ and $E_{a,i} = 150$ μJ. (b) Dependence of G and γ on the intersection angle of the laser beams. Closed circles: $E_{a,i} = 80$ μJ, $E_{d,i} = 840$ μJ, s polarization; open circles: $E_{a,i} = 80$ μJ, $E_{d,i} = 840$ μJ, p polarization; squares: $E_{a,i} = 80$ μJ, $E_{d,i} = 810$ μJ, p polarization. The squares were measured using longer focal length lenses (300 mm for the donor and 200 mm for the acceptor). (c) Donor (open symbols) and acceptor (solid symbols) output energies vs pulse delay, with $E_{d,i} = 820$ and $E_{a,i} = 150$ μJ.

We find quantitative energy transfer from the donor to the acceptor when the pulses are temporally overlapped, with a FWHM of 110 fs. This width equals the overlap time of the two pulses, corresponding to an overlap distance of 33 μm.

A key to understanding the energy transfer mechanism is the change in the spectral bandwidth of the lasers produced by the plasma. Figure 4(a) shows the spectrum of the acceptor laser before and after the focus, the latter with and without the donor beam present. We see that without

the donor the acceptor pulse is broadened [16,17] and blueshifted [18,19] out to 700 nm. In the presence of the donor the acceptor pulse shows enhanced amplification at short wavelengths. We also observed a third harmonic generation efficiency of 2.5×10^{-5} when the pulses overlapped temporally, with $E_{a,i} = 6$ and $E_{d,i} = 610$ μJ. Figure 4(b) shows the far field donor spectrum, measured with and without the acceptor pulse. Figure 4(c) shows that the temporal width of the acceptor pulse is compressed up to 50%, from 52 to 27 fs, as its initial energy is increased from 6 to 31 μJ.

A mechanism that explains our observations is stimulated Raman scattering by a plasma [20,21]. In plasma-mediated SRS, the electromagnetic fields of the donor and acceptor (known as the ''pump'' and ''seed'' in the Raman literature) lasers are coupled by an electrostatic plasma wave. In the linear regime, Stokes and anti-Stokes photons generated from the noise are amplified and scattered into the acceptor without depleting the donor. In the nonlinear regime, photons are transferred from the donor to the acceptor, with the energy difference between the incident and scattered photons taken up or provided by the plasma [22].

Necessary conditions for SRS are (i) an under dense plasma with $n_e < n_{cr}/4$, where n_e is the electron density and n_{cr} is the critical density for laser frequency ω, (ii) conservation of energy, $\omega_p = \omega_s \pm \omega_{pe}$, where ω_p and ω_s are the angular frequencies of the pump and seed lasers, and ω_{pe} is the plasma frequency at density n_e, and (iii) conservation of momentum, $\mathbf{k_p} = \mathbf{k_s} \pm \mathbf{k_{pe}}$, where $\mathbf{k_i}$ are wave vectors and the $\pm$ signs are for Stokes and anti-Stokes scattering, respectively [20]. The spectra in Fig. 3(b) show that anti-Stokes scattering dominates. Here, $n_e < 0.01 n_{cr}$, condition (ii) is satisfied by the supercontinuum, as explained later, and condition (iii) determines the angular dependence of the amplification ratio.

Stimulated Raman scattering in a plasma, which is generally carried out using either forward or backwards scattering, has been exploited as a promising technique to amplify high intensity ultrashort laser pulses [12]. In the forward configuration, short pump and seed pulses copropagate; as they travel forward, the two pulses interact nonlinearly until they are separated by dispersion-induced walk-off. In the backwards configuration, a short seed pulse counter-propagates through a long pump pulse, drawing energy from it as it passes through [23]. In Raman laser amplifiers the latter configuration is employed because the transfer of energy from a long to a short pulse can produce a large increase in the seed intensity [24]. Plasma amplifiers typically use a ns laser to create the plasma, a long (~20 ps) Ti:sapphire laser pulse for the pump, and a shorter (~0.5 ps) Ti:sapphire laser pulse for the seed [12]. The frequency of the seed is tuned with a Raman shifter or an optical parametric amplifier to satisfy the frequency matching condition. Such devices, when operating in the linear regime, produce little or no pump depletion [25], and even in the nonlinear regime only 4% depletion has been observed in a single pass [12]. Amplification by backwards SRS is limited by the low average pump depletion rate and saturation of the seed energy, which are attributed mainly to the poor mismatch between the pump and seed bandwidths [22,26]. The present results suggest that some of these limitations may be overcome by forward scattering.

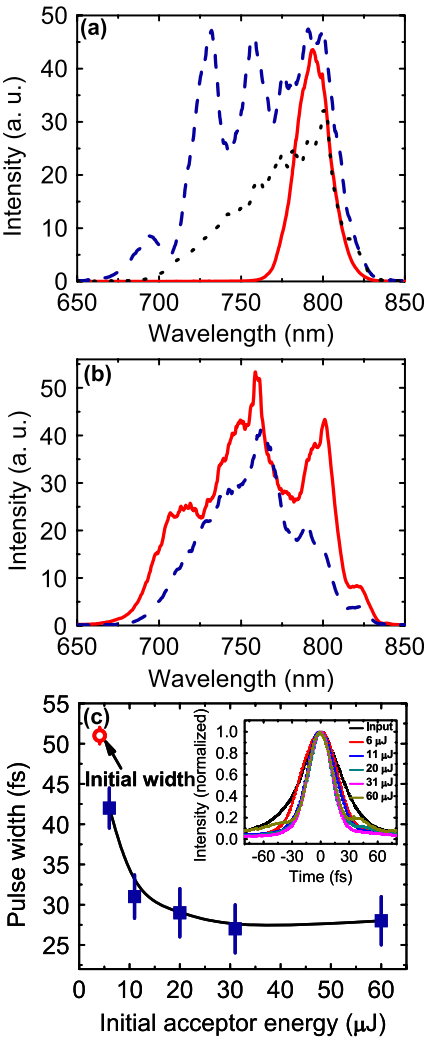

FIG. 4 (color online). Spectral and temporal properties of the donor and acceptor pulses. (a) Spectral profile of the acceptor pulse, measured before the laser focus (solid curve), after the laser focus with (dashes) and without (dots) the donor pulse, respectively. (b) Spectral profile of the donor pulse measured after the laser focus with (dashes) and without (solid curve) the acceptor pulse. In both panels, $E_{d,i} = 840$ and $E_{a,i} = 160$ μJ. (c) Temporal widths of the amplified acceptor pulses for different initial acceptor pulse energies with $E_{d,i} = 840$ μJ. The inset shows the autocorrelation curves from which the pulse widths were determined. In all three panels, the beams are s polarized with an intersection angle of 30°.

Highly efficient SRS in the forward direction has been achieved in liquids by generating nonlinear conical

X waves in both the pump and Raman-shifted pulses [27]. High conversion efficiency is possible because the conical wave split off from the Raman pulse, generated either spontaneously or from a seed pulse, is slaved to travel with the same group velocity as its pump counterpart. Another means of transferring energy in the forward direction is scattering from a dynamical grating formed in the filaments of two lasers intersecting at a grazing angle [14]. Plasma formation is not required, and symmetry breaking is caused by time ordering and relative chirp of the two beams. This is a relatively inefficient process, with a maximum of $D = 7\%$ having been reported in air [14].

In the present experiment the donor and acceptor lasers start out with identical bandwidths. Efficient energy transfer is possible because of the spectral modifications caused by blueshifting and supercontinuum generation (SCG) in the plasma. The plasma density (measured interferometrically) of $\sim 5.3 \times 10^{18}$ cm^{-3} in Fig. 4 produces a frequency shift $\omega_p - \omega_s$ corresponding to a wavelength difference between the pump and seed pulses of ~ 38 nm. As seen in Fig. 4(a), this difference matches the blueshift of the center of the acceptor spectrum with respect to the peak wavelength of the unperturbed laser. Symmetry breaking, causing one laser to be the donor and the other the acceptor, is the result of blueshifting in the intersection region, which occurs after the focal point of the acceptor laser. For anti-Stokes scattering the blueshifted laser becomes the acceptor.

A key issue is the angular dependence of the energy transfer rate. The dispersion relations for an underdense plasma [20] predict forward and backward growth rates of $\gamma_f = 0.04$ ps^{-1} and $\gamma_b = 7$ ps^{-1}. (The growth rate is related to the gain ratio by $G = \exp(\gamma d/c \sin\theta)$, where d is the beam diameter and c is the speed of light, assuming simple geometric optics in the intersection region.) The falloff in G and γ vs θ may be explained by Landau damping, which occurs away from the forward direction. An analytical model [28] predicts a maximum in γ at $\theta = 30°$, in agreement with Fig. 3(b).

The dependence of the energy transfer on the polarization angle may be explained by assuming that the growth rate is proportional to the square of the dot product of the donor and acceptor electric fields. The curve in Fig. 3(a) was calculated by solving the field coupling equations in the steady state limit [11].

In conclusion, we have shown that very large donor depletion in a near-forward direction is made possible by blueshifting and SCG. The very high transfer efficiencies are attributed to at least three factors: (i) spectral modifications of the acceptor, which provide the necessary frequency matching for energy conservation, (ii) efficient near-forward scattering, where Landau damping does not limit the growth rate, and (iii) sufficient acceptor energy to deplete the donor pulse. The present experiments were performed in air, and it is likely that a higher energy transfer ratio is achievable in different gaseous media and at different pressures. The achievement of high SRS energy transfer on small spatial (within tens of μm) and temporal (tens of fs) scales make it feasible to build fast miniature photonic devices. This proof of principle could potentially lead to the construction of all-optical switches, filters, modulators, and wavelength converters in bulk materials having strong Raman activity.

The authors wish to thank Professor T. Seideman and Professor Y. Prior for fruitful discussions, and the University of Illinois at Chicago for financial support.

[1] D. R. Solli, C. Ropers, and B. Jalali, Phys. Rev. Lett. **101**, 233902 (2008).
[2] X. Li *et al.*, Science **301**, 809 (2003).
[3] J. L. O'Brien *et al.*, Nature (London) **426**, 264 (2003).
[4] S. L. Neale *et al.*, Nature Mater. **4**, 530 (2005).
[5] T. Tanabe *et al.*, Appl. Phys. Lett. **87**, 151112 (2005).
[6] M. Peccianti *et al.*, Appl. Phys. Lett. **81**, 3335 (2002).
[7] R. J. Gordon *et al.*, J. Appl. Phys. **94**, 669 (2003).
[8] M. A. Duguay and J. W. Hansen, Appl. Phys. Lett. **15**, 192 (1969).
[9] K.-J. Boller, A. Imamoğlu, and S. E. Harris, Phys. Rev. Lett. **66**, 2593 (1991).
[10] L. V. Hau *et al.*, Nature (London) **397**, 594 (1999).
[11] R. Shen, *Principles of Nonlinear Optics* (Wiley-Interscience, Hoboken, 2003).
[12] J. Ren *et al.*, Phys. Plasmas **15**, 056702 (2008).
[13] P. A. Agrawal, *Nonlinear Fiber Optics* (Academic Press, San Diego, 2001).
[14] A. C. Bernstein, M. McCormick, G. M. Dyer, J. C. Sanders, and T. Ditmire, Phys. Rev. Lett. **102**, 123902 (2009).
[15] A. A. Balakin *et al.*, JETP Lett. **80**, 12 (2004).
[16] R. R. Alfano, *The Supercontinuum Laser Source* (Springer-Verlag, New York, 1989).
[17] P. B. Corkum, C. Rolland, and T. Srinivasan-Rao, Phys. Rev. Lett. **57**, 2268 (1986).
[18] E. Yablonovitch, Phys. Rev. A **10**, 1888 (1974).
[19] W. M. Wood, C. W. Siders, and M. C. Downer, Phys. Rev. Lett. **67**, 3523 (1991).
[20] W. M. Kruer, *The Physics of Laser Plasma Interactions* (Westview Press, Boulder, 2003).
[21] H. A. Baldis, E. M. Campell, and W. L. Kruer, in *Handbook of Plasma Physics*, edited by M. N. Rosenbluth and R. Z. Sagdeev (Elsevier, Amsterdam, 1991), Vol. 3.
[22] W. Cheng *et al.*, Phys. Rev. Lett. **94**, 045003 (2005).
[23] J. R. Murray *et al.*, IEEE J. Quantum Electron. **15**, 342 (1979).
[24] N. J. Fisch, and V. M. Malkin, Phys. Plasmas **10**, 2056 (2003).
[25] Y. Ping, I. Geltner, A. Morozov, N. J. Fisch, and S. Suckewer, Phys. Rev. E **66**, 046401 (2002).
[26] J. Ren *et al.*, Nature Phys. **3**, 732 (2007).
[27] D. Faccio *et al.*, Opt. Express **15**, 13 077 (2007).
[28] S. C. Wilks *et al.*, Phys. Fluids B **4**, 2794 (1992).